

See discussions, stats, and author profiles for this publication at: <https://www.researchgate.net/publication/265377649>

Accurate Identification and Selective Removal of Rotavirus Using a Plasmonic–Magnetic 3D Graphene Oxide Architecture

ARTICLE in JOURNAL OF PHYSICAL CHEMISTRY LETTERS · SEPTEMBER 2014

Impact Factor: 7.46 · DOI: 10.1021/jz501402b

CITATIONS

4

READS

87

10 AUTHORS, INCLUDING:



[Brian G Yust](#)

University of Texas Rio Grande Valley

31 PUBLICATIONS 93 CITATIONS

[SEE PROFILE](#)



[Avijit Pramanik](#)

Jackson State University

53 PUBLICATIONS 405 CITATIONS

[SEE PROFILE](#)



[Suhash Chavva](#)

Jackson State University

14 PUBLICATIONS 34 CITATIONS

[SEE PROFILE](#)



[Dhiraj K Sardar](#)

University of Texas at San Antonio

263 PUBLICATIONS 1,840 CITATIONS

[SEE PROFILE](#)

Accurate Identification and Selective Removal of Rotavirus Using a Plasmonic–Magnetic 3D Graphene Oxide Architecture

Zhen Fan,[†] Brian Yust,[‡] Bhanu Priya Viraka Nellore,[†] Sudarson Sekhar Sinha,[†] Rajashekhar Kanchanapally,[†] Rebecca A. Crouch,[†] Avijit Pramanik,[†] Suhash Reddy Chavva,[†] Dhiraj Sardar,[‡] and Paresh Chandra Ray^{*,†}

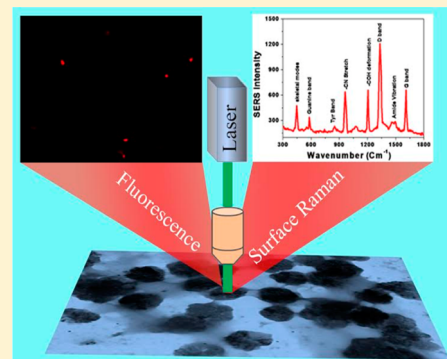
[†]Department of Chemistry and Biochemistry, Jackson State University, Jackson, Mississippi 39217, United States

[‡]Department of Physics and Astronomy, University of Texas at San Antonio, San Antonio, Texas 78249, United States

Supporting Information

ABSTRACT: According to the World Health Organization, even in the 21st century, more than one million children die each year due to the rotavirus contamination of drinking water. Therefore, accurate identification and removal of rotavirus are very important to save childrens' lives. Driven by the need, in this Letter, we report for the first time highly selective identification and removal of rotavirus from infected water using a bioconjugated hybrid graphene oxide based three-dimensional (3D) solid architecture. Experimental results show that due to the presence of a high intensity of "hot spots" in the 3D network, an antibody-attached 3D plasmonic–magnetic architecture can be used for accurate identification of rotavirus using surface-enhanced Raman spectroscopy (SERS). Reported data demonstrate that the antibody-attached 3D network binds strongly with rotavirus and is capable of highly efficient removal of rotavirus, which has been confirmed by SERS, fluorescence imaging, and enzyme-linked immunosorbent assay (ELISA) data. We discuss a possible mechanism for accurate identification and efficient removal of rotavirus from infected drinking water.

SECTION: Plasmonics, Optical Materials, and Hard Matter



According to the World Health Organization (WHO), more than 1.1 billion people have no access to quality drinking water that is free from rotavirus contamination even today.^{1,2} As a result, more than 1.5 million children die each year due to rotavirus contamination.^{1–4} Therefore, accurate detection and removal of rotavirus are very important to save childrens' lives in our society. Driven by need, in this Letter, we report for the first time a highly selective rotavirus identification as well as removal from a water sample using plasmonic–magnetic hybrid graphene oxide based three-dimensional (3D) solid architectures, as shown in Scheme 1. 3D graphene oxide architectures were developed from magnetic core–plasmonic shell nanoparticle-attached 2D graphene oxide using poly(ethylene glycol) (PEG), as shown in Figure 1A.

Due to the low cost, high yield, easy production, and interesting properties, graphene oxide holds great promise for daily life applications.^{5–14} In 2D graphene oxide, functional oxygen groups serve as anchoring points for developing a 3D architecture,^{15–23} which can have tremendous practical applications. In this Letter, we have shown that bioconjugated graphene oxide based 3D architectures can be used for the selective identification and removal of rotavirus from a water sample. PEG is well-known for biocompatible and non-immunogenic materials,⁴ and as a result, in our design, we have used PEG as a stabilizer and a cross-linking agent. In our

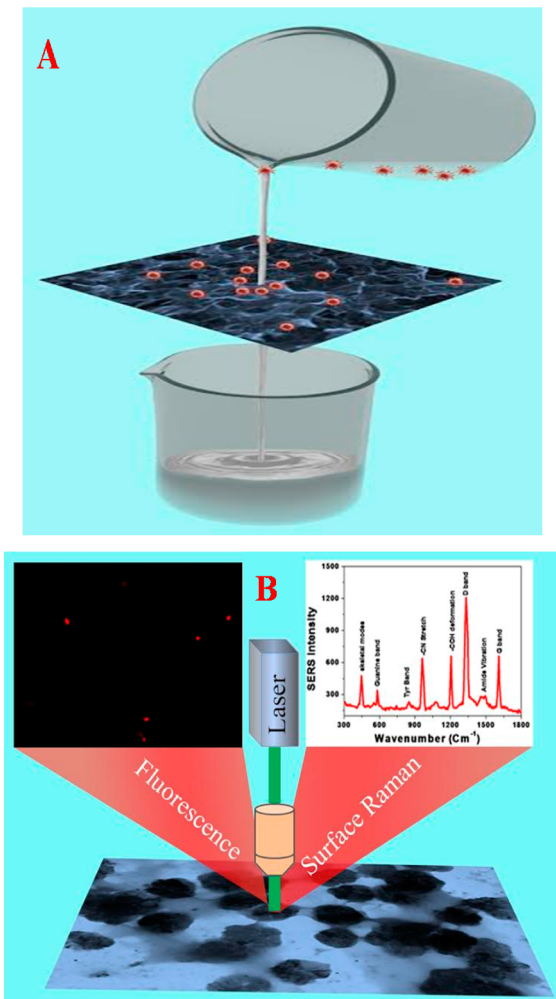
design, the 3D macroporous network offers a large surface area for the effective binding of rotavirus via antibody. Also, a highly porous structure with pore sizes of several micrometers, as shown in Figure 2A, helps to remove bacteria from the water sample via diffusion/adsorption. Magnetic properties of the iron oxide magnetic core nanoparticle-attached^{24–28} 3D graphene oxide foam have been used for removal of rotavirus. On the other hand, plasmonic properties of a gold shell nanoparticle-attached 3D architecture has been used for the detection of microbes selectively using surface-enhanced Raman spectroscopy (SERS).^{29–37} SERS is known to be useful as a whole-organism fingerprint,^{24,38,39} and as a result, here we have used a 3D graphene oxide based SERS technique for the characterization and accurate identification of rotavirus.

To develop a 3D plasmonic–magnetic architecture, initially, iron oxide core–plasmonic gold shell nanoparticles were synthesized in the presence of iron nanoparticle, gold chloride (HAuCl_4), trisodium citrate, and sodium borohydride using our reported synthesis procedure.^{24,25} Next, we modified the nanoparticle surface by amine groups using cystamine dihydrochloride. After that, core–shell nanoparticle-attached

Received: July 6, 2014

Accepted: September 4, 2014

Scheme 1. (A) Schematic Representation Showing the Rotavirus Separation Capability Using a 3D Plasmonic–Magnetic Graphene Oxide Architecture and (B) Schematic Representation Showing That Antibody-Bound 3D Graphene Oxide Can Be Used for SERS and Fluorescence Imaging of Rotavirus after Separation



2D graphene oxide was synthesized. Details of the synthesis procedure for 2D graphene oxide attached core–shell nanoparticle are reported in the Supporting Information. At the end, the 3D plasmonic–magnetic architecture was developed using PEG (average $M_n = 400$) as a cross-linking agent, as shown in Figure 1A. We used coupling chemistry between the $-\text{NH}_2$ group of the nanoparticle and the $-\text{OH}$ group of PEG to form a 3D material from 2D hybrid graphene oxide. At the end, solid product was dried to form a product, as shown in Figure 1A, and was used for further characterization. The size of the 3D architecture was about 1 in. in width and 1.5 in. in length, as shown in Figure 1A.

The FT-IR spectrum of the 3D hybrid graphene oxide network in Figure 1C shows a vibrational peak at $\sim 3034 \text{ cm}^{-1}$, which is due to the formation of hydrogen bonds between the $-\text{NH}_2/\text{NH}$ groups of amine-functionalized core–shell nanoparticles and the $-\text{OH}$ groups of PEG. Similarly, the strong peak at $\sim 1680 \text{ cm}^{-1}$ corresponds to the vibrational mode of the carbonyl ($-\text{C}=\text{O}$) groups due to the graphene oxide. Also, peaks were observed at $\sim 1725 \text{ cm}^{-1}$ for the carbonyl ($-\text{C}=\text{O}$) stretch of carboxylic acid and at $\sim 3780 \text{ cm}^{-1}$ due to $-\text{OH}$

groups. Additionally, a vibrational peak was observed for $-\text{NCO}$ vibrations at $\sim 2270 \text{ cm}^{-1}$. Similarly, two bands ~ 3250 and $\sim 3360 \text{ cm}^{-1}$ are due to the $-\text{NH}$ group in the amine-functionalized nanoparticle. Figure 1B displays the Hitachi S5500 ultra-high-resolution SEM image of the 3D microstructure, which shows an interconnected 3D network with a pore size of 5–10 μm .

The EDX mapping in S. Figure 3 in the Supporting Information clearly shows the presence of Fe and Au with C and O in the 3D hybrid graphene oxide network. Using nitrogen adsorption analysis via the Brunauer–Emmett–Teller method, it was found that the specific surface area for the 3D magnetic hybrid architecture was $420 \text{ m}^2 \text{ g}^{-1}$, and the pore volume was $0.620 \text{ cm}^3 \text{ g}^{-1}$. SQID measurements indicated that the 3D architecture showed ferromagnetic behavior with saturation magnetization of 53.2 emu g^{-1} . Figure 1E shows the broad and structureless absorption spectrum of 2D graphene oxide. Observed structureless absorption behavior for 2D graphene oxide is mainly due to E_{11} and E_{22} transitions,^{6–13} which occur between the first and second singularities located around the Fermi level. In the case of the 3D architecture, a quite broad plasmon peak was observed starting at around 550 nm. This strong long-wavelength plasmon band is due to the oscillation of the conduction band electrons of the core–shell nanoparticles, as we have previously reported.^{24,25} Because in the 3D hybrid network the core–shell nanoparticles are in close contact, the plasmon band becomes very broad, absorbing from 550 to 850 nm wavelengths and indicating a certain degree of aggregation, which results in conditions conducive to the formation of “hot spots” that provide significant Raman signal enhancement. Figure 1D shows the Raman spectrum of graphene oxide, which clearly shows the D band at 1342 cm^{-1} and a G band at 1614 cm^{-1} .^{6–13} The observed strong D band in the SERS spectra clearly indicates that the degree of oxidation is high.

Next, the plasmonic–magnetic 3D architectures were tested for their ability to be utilized in the separation, detection, and removal of rotavirus from water. Because the anti-rotavirus antibody is known to be selective for rotavirus,³⁸ this monoclonal antibody (purchased from Abcam (ab130835, www.abcam.com)) was attached via the amine group of the magnetic–plasmonic nanoparticles already bound to modified graphene oxide. Similarly, the monoclonal antibody was also attached with graphene oxide via the primary amines group of the antibody. Thus, the monoclonal antibody-attached 3D architecture was developed, where antibodies are attached with graphene oxide as well as with core–shell nanoparticles. To test the removal capability via attachment and absorption, the anti-rotavirus antibody-attached 3D solid architecture was added to a 100 mL water sample containing 5.9×10^5 plaque-forming units (PFU)/mL of rotavirus. The flask containing this rotavirus-infected water sample and the solid plasmonic–magnetic 3D architecture was shaken in a rotary shaker for 40 min. Following incubation, the 3D architecture containing adsorbed rotavirus was separated from the water sample using a bar magnet. After that, the reverse transcription polymerase chain reaction (RT-PCR)^{40,41} was used to detect the amount of rotavirus remaining in the water sample. The characterization was carried out using TEM, fluorescence imaging, and SERS for the rotavirus on the 3D architecture. The TEM image reported in Figure 2A clearly shows that rotavirus is attached to the surface of the 3D architecture. Figure 2E,F shows that the 3D network was able to absorb and remove more than 99%

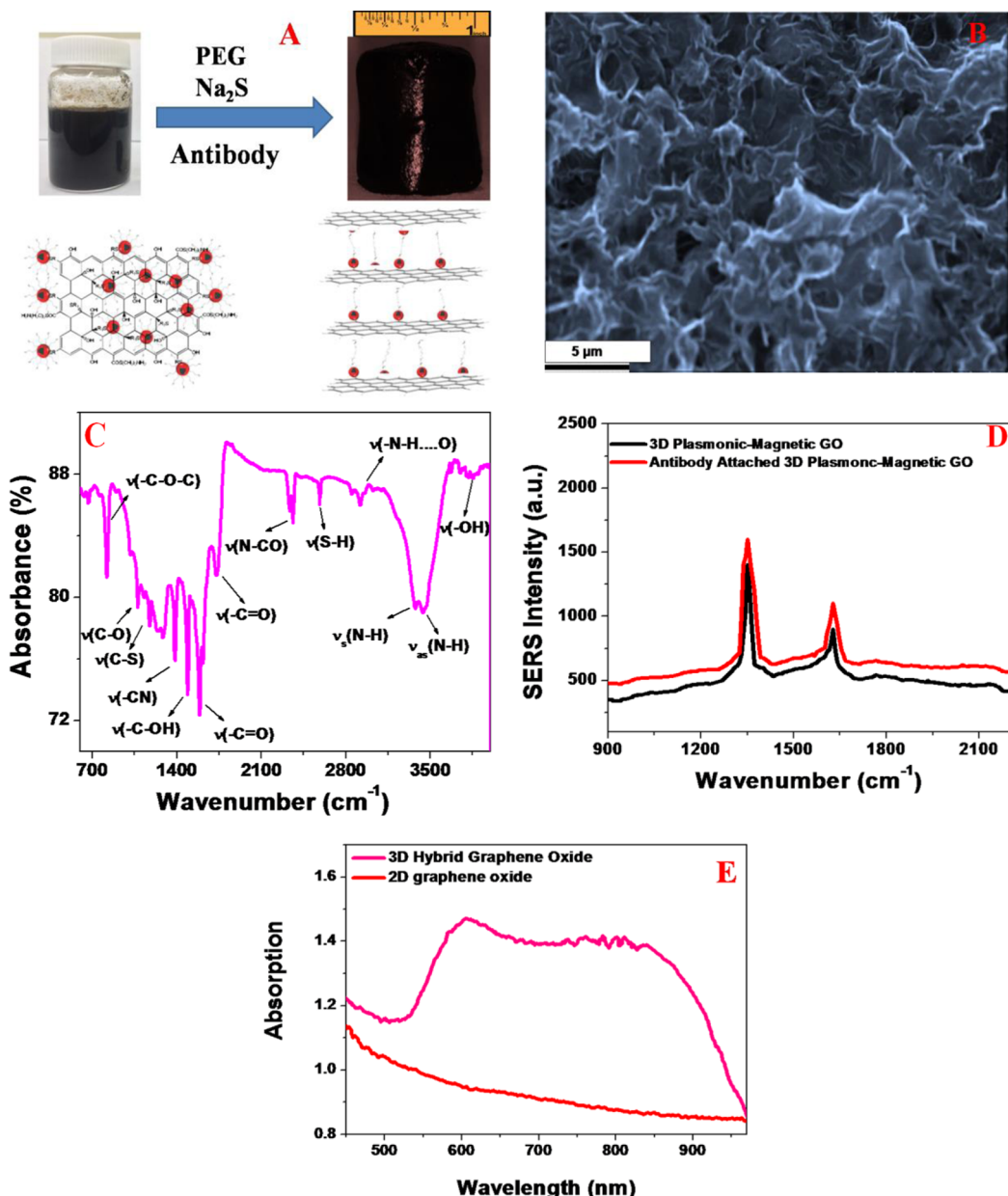


Figure 1. (A) Photograph showing the formation of a plasmonic–magnetic 3D hybrid graphene oxide architecture. For the development of the 3D architecture, 2D graphene oxide sheets were self-assembled using PEG. (B) SEM image of a 3D architecture showing an interconnected 3D network with a pore size of several microns. (C) FT-IR spectrum from macroscopic network verifying the existence of hydrogen bonding, $-\text{CO}$, $-\text{OH}$, $-\text{CN}$, and $-\text{NH}$ groups. (D) SERS spectra clearly showing the presence of D and G bands for only plasmonic–magnetic graphene oxide and antibody-attached plasmonic–magnetic graphene oxide. (E) Extinction spectra of 2D graphene oxide before core–shell nanoparticles were attached and that of a 3D hybrid graphene oxide network.

rotavirus from a water sample within 40 min when the initial concentration of rotavirus was 5.9×10^5 PFU/mL. This highly efficient rotavirus removal performance using the novel 3D architecture is due to the following factors. The anti-rotavirus antibody binds strongly with rotavirus and can remove the virus from the water sample during magnetic separation, and the 3D plasmonic–magnetic architecture contains a highly open pore network with pore sizes between 5 and 10 μm , which facilitates fast diffusion of rotavirus (~ 100 nm size) into the interior of the 3D network. For better understanding, we have also performed fluorescence imaging. For this purpose, methylene-blue-modified anti-rotavirus antibody was attached to the 3D network. The fluorescence images in Figure 2B,C also show

that the rotavirus was present on the surface of the 3D architecture after it was immersed in the rotavirus-infected water sample. On the other hand, no fluorescence was observed from the water sample after magnetic separation.

As we have discussed before, 3D organization of the nanostructure developed by us can be an excellent SERS substrate. It is due to the presence of high-intensity hot spots, which amplify the SERS signal tremendously. Also, in our 3D hybrid architecture, graphene oxide enhances the SERS signal via chemical enhancement, and the plasmonic gold nano-assembly enhances the SERS signal via electromagnetic enhancement. As a result, very high sensitivity can be obtained for the specific virus detection. SERS experiments were

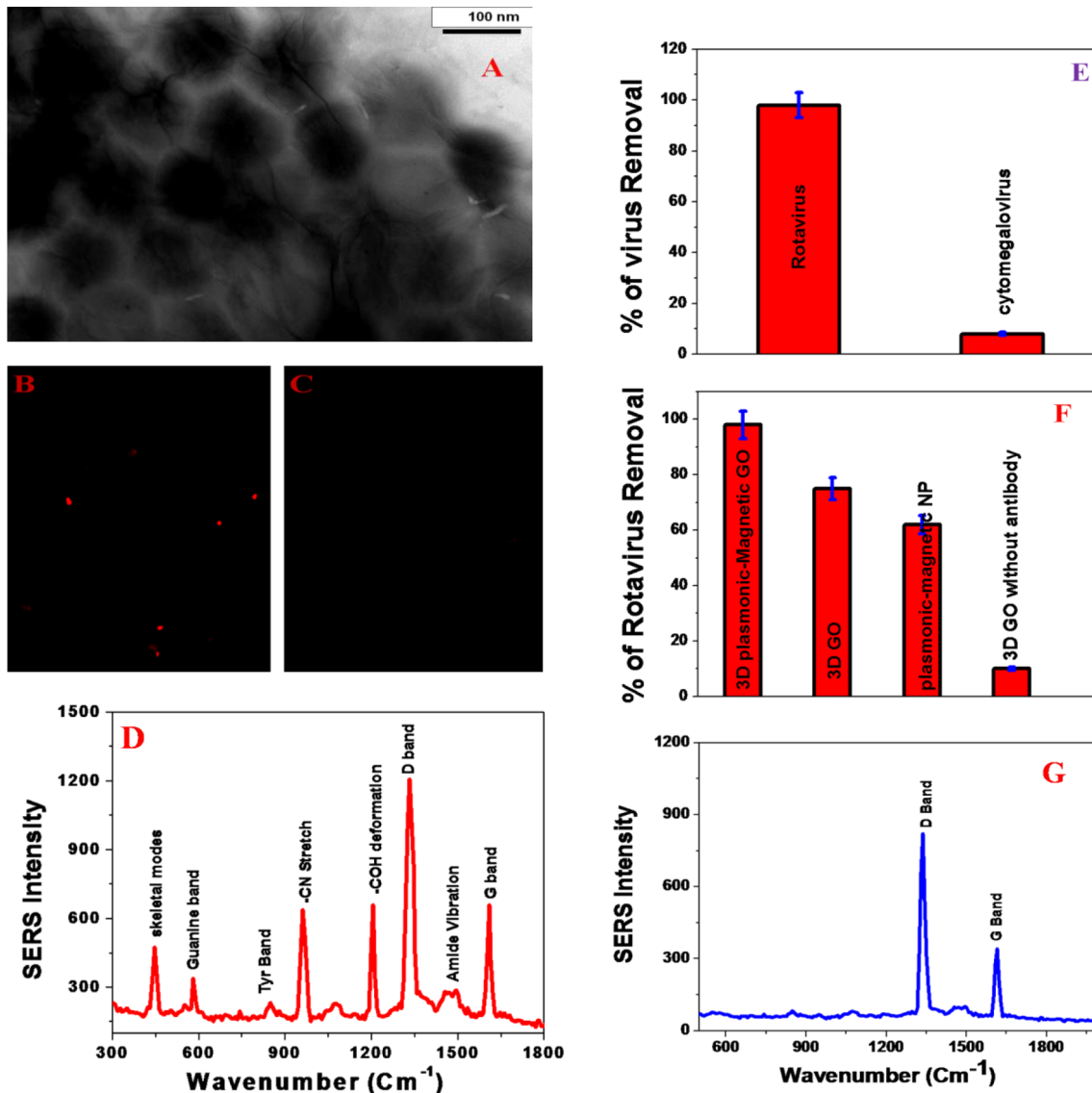


Figure 2. (A) TEM image demonstrating binding of rotavirus onto the 3D hybrid architecture. (B,C) Fluorescence images of rotavirus. Panel (B) shows the presence of rotavirus separated by attachment to the 3D architecture via the anti-rotavirus antibody. Panel (C) shows the absence of rotavirus in a previously infected water sample after 45 min of incubation with the 3D architecture. (D) SERS intensity from rotavirus conjugated to the 3D architecture after magnetic separation. The observed SERS signal is directly from the rotavirus. No SERS signal was observed from water after magnetic separation. (E) Plot showing selective rotavirus removal using anti-rotavirus antibody-attached 3D plasmonic–magnetic hybrid graphene oxide after 40 min of incubation. RT-PCR was used to quantify the amount of rotavirus present. (F) Plot shows rotavirus removal efficiency for 3D plasmonic–magnetic hybrid graphene oxide with and without antibody, 3D graphene oxide with antibody and core–shell nanoparticle with antibody. RT-PCR was used to quantify the amount of rotavirus present. (G) Spectrum showing the SERS intensity from the 3D architecture after incubation with cytomegalovirus (CMV) for 40 min followed by magnetic separation. The observed SERS signal is directly from the graphene oxide.

performed to determine whether 3D architecture-based SERS could be used for rotavirus identification. Figure 2D shows the SERS spectrum for the rotavirus-attached 3D network after magnetic separation. The strongest Raman bands seemed to consist of the graphene oxide D and G bands. Other prominent bands are mainly due to the protein backbone amide I and $-\text{COH}$ deformation bands, the guanine band, the skeletal vibrations, and the bands of fatty acids.³⁹ In the SERS spectrum, the Raman band at $\sim 595 \text{ cm}^{-1}$ is due to the guanine. The band at $\sim 1210 \text{ cm}^{-1}$ is due to the $-\text{COH}$ deformation band of proteins. Additionally, the $\sim 1047 \text{ cm}^{-1}$ band is due to $\nu(\text{C}-\text{N})$ from amino acids. Observed vibrational modes are in good agreement with the Raman bands reported for the rotavirus in the literature.³⁹ As shown in Figure 1D, the

SERS spectrum from the antibody-attached 3D network exhibits only graphene oxide D and G bands. From Figures 1D and 2D, we can conclude that excess Raman bands observed as shown in Figure 2D are mainly from rotavirus.

Figure 2F shows how capture efficiency varies for the antibody-attached 3D architecture with a plasmonic–magnetic nanoparticle, antibody-attached 3D graphene oxide without a plasmonic–magnetic nanoparticle, the antibody-attached plasmonic–magnetic nanoparticle, and 3D graphene oxide without the antibody. In each case, after 40 min of incubation, we used RT-PCR to detect the amount of rotavirus remaining in the water sample. Our results clearly show that the capture efficiency is maximum, which is around 99%, in the case of the antibody-attached plasmonic–magnetic nanoparticle-bound 3D

architecture, whereas the capture efficiency was less than 75% when the antibody-attached 3D graphene oxide or antibody-attached core–shell nanoparticle was used. On the other hand, around 10% capture efficiency was observed in the case of 3D graphene oxide without the antibody after 40 min of incubation. The above 10% capture by 3D graphene oxide without the antibody is mainly due to the diffusion of rotavirus into the interior of the 3D network. All of the above data clearly show that most of the rotavirus was removed due to binding with anti-rotavirus antibody.

Next, to understand how selective the 3D architecture is for capture and accurate identification of rotavirus, we have also performed the same experiment with cytomegalovirus (CMV). For this purpose, the anti-rotavirus antibody-attached 3D solid architecture was added into a 100 mL water sample containing 6.2×10^5 PFU/mL of CMV. After that, the mixture was shaken in a rotary shaker for 40 min and then separated using a bar magnet. After that, RT-PCR was used to detect the amount of CMV remaining in the water sample. Figure 2E clearly shows that the capture efficiency is only 8% for CMV, whereas the capture efficiency was more than 99% in the case of rotavirus. The 8% CMV captured by anti-rotavirus antibody-attached 3D graphene oxide is mainly due to the diffusion of CMV into the interior of the 3D network. Figure 2G shows the SERS spectra from anti-rotavirus antibody-attached 3D graphene oxide after incubation with 6.2×10^5 PFU/mL of CMV for 40 min and then separation by a magnet. In the SERS spectra, we have observed only D and G bands from graphene oxide, and no SERS peak was observed from the virus, whereas, as shown Figure 2D, in the case of rotavirus, we have observed several Raman peaks from the virus. This is due to the fact that in the case of rotavirus, after separation, rotaviruses are mainly attached onto the surface of the 3D architecture via the antibody, and as a result, we have observed a huge SERS peak from the virus. On the other hand, in the case of CMV, few CMVs are captured into the interior of the 3D network, and these are not well exposed to laser light during SERS measurement. As a result, we are not able to observe any Raman peaks from the virus. All of the above experimental data clearly show that the anti-rotavirus antibody-attached 3D plasmonic–magnetic architecture can be used for the separation and accurate identification of rotavirus.

In conclusion, in this Letter, we have reported selective detection and complete removal of rotavirus from water samples using a 3D plasmonic–magnetic solid architecture. We have used H₂N-PEG-NH₂ coupling chemistry to form the 3D plasmonic–magnetic architecture from magnetic nanoparticle-attached 2D hybrid graphene oxide. We have shown that the plasmonic 3D network is very useful for SERS imaging for rotavirus identification. Our experimental results with rotavirus and CMV show that the antibody-attached 3D network binds strongly with rotavirus and removes them from the water sample. Both SERS and fluorescence imaging with RT-PCR data confirm our results. Our experimental data based on the 3D plasmonic–magnetic architecture reported here open up a new possibility for rapid, label-free identification and highly efficient removal of rotavirus from environmental samples. Though we have used the antibody-functionalized core–shell nanoparticle-attached 3D graphene oxide, one may be able to use another antibody-functionalized core–shell nanoparticle-attached porous membrane sheet with the same porosity for rotavirus separation.

ASSOCIATED CONTENT

Supporting Information

Detailed synthesis and characterization of the 3D hybrid graphene oxide architecture and other experiments are available. This material is available free of charge via the Internet at <http://pubs.acs.org>.

AUTHOR INFORMATION

Corresponding Author

*E-mail: paresh.c.ray@jsums.edu. Fax: +16019793674.

Notes

The authors declare no competing financial interest.

ACKNOWLEDGMENTS

Dr. Ray thanks NSF-PREM Grant # DMR-1205194 for their generous funding. Dr. Sardar thanks the NSF-PREM Grant # DMR-0934218 for their generous funding.

REFERENCES

- (1) Health through safe drinking water and basic sanitation. http://www.who.int/water_sanitation_health/mdg1/en/ (date of access 10/12/2013).
- (2) Liu, C.; Xie, X.; Zhao, W.; Liu, N.; Maraccini, P. A.; Sassoubre, L. M.; Boehm, A. B.; Cui, Y. Conducting Nanospunge Electroporation for Affordable and High-Efficiency Disinfection of Bacteria and Viruses in Water. *Nano Lett.* **2013**, *13*, 4288–4293.
- (3) Qu, X.; Brame, J.; Li, Q.; Alvarez, P. J. J. Nanotechnology for Safer Water Supply: Enabling Integrated Water Treatment and Reuse. *Acc. Chem. Res.* **2013**, *46*, 834–843.
- (4) Hak, S.; Helgesen, E.; Hektoen, H. H.; Huuse, E. M.; Jarzyna, P. A.; Mulder, W. J.; Haraldseth, O.; Davies, C. L. The Effect of Nanoparticle Polyethylene Glycol Surface Density on Ligand-Directed Tumor Targeting Studied *In Vivo* by Dual Modality Imaging. *ACS Nano* **2012**, *6*, 5648–5658.
- (5) Hummers, W. S.; Offeman, R. E. Preparation of Graphitic Oxide. *J. Am. Chem. Soc.* **1958**, *80*, 1339.
- (6) Geim, A. K.; Novoselov, K. S. The Rise of Graphene. *Nat. Mater.* **2007**, *6*, 183–191.
- (7) Lightcap, I. V.; Kamat, P. V. Graphitic Design: Prospects of Graphene-Based Nanocomposites for Solar Energy Conversion, Storage, and Sensing. *Acc. Chem. Res.* **2013**, *46*, 2235–2243.
- (8) Kamat, P. V. Graphene-Based Nanoarchitectures. Anchoring Semiconductor and Metal Nanoparticles on a Two-Dimensional Carbon Support. *J. Phys. Chem. Lett.* **2010**, *1*, 520–527.
- (9) Fan, Z.; Kanchanapally, R.; Ray, P. C. Hybrid Graphene Oxide Based Ultrasensitive SERS Probe for Label-Free Biosensing. *J. Phys. Chem. Lett.* **2013**, *4*, 3813.
- (10) Kanchanapally, R.; Sinha, S. S.; Fan, Z.; Dubey, M.; Zakar, E.; Ray, P. C. Graphene Oxide–Gold Nanocage Hybrid for Trace Level Identification of Nitro Explosives Using Raman Fingerprint. *J. Phys. Chem. C* **2014**, *4*, 7070–7075.
- (11) Loh, K. P.; Bao, Q.; Eda, G.; Chowalla, M. Graphene Oxide As a Chemically Tunable Platform for Optical Applications. *Nat. Chem.* **2010**, *2*, 1015–1024.
- (12) Pramanik, A.; Chavva, S. R.; Fan, Z.; Sinha, S.; Nellore, B. P.; Ray, P. C. Extremely High Two-Photon Absorbing Graphene Oxide for Imaging of Tumor Cells in the Second Biological Window. *J. Phys. Chem. Lett.* **2014**, *5*, 2150–2154.
- (13) Castro Neto, A. H.; Guinea, F.; Peres, N. M. R.; Novoselov, K. S.; Geim, A. K. The Electronic Properties of Graphene. *Rev. Mod. Phys.* **2009**, *81*, 109–111.
- (14) Kim, D. W.; Kim, Y. H.; Jeong, H. S.; Jung, H.-T. Direct Visualization of Large-Area Graphene Domains and Boundaries by Optical Birefringency. *Nat. Nanotechnol.* **2012**, *7*, 29–34.
- (15) Wu, Z. S.; Yang, S.; Sun, Y.; Parvez, K.; Feng, X.; Müllen, K. 3D Nitrogen-Doped Graphene Aerogel-Supported Fe₃O₄ Nanoparticles as

- Efficient Electrocatalysts for the Oxygen Reduction Reaction. *J. Am. Chem. Soc.* **2012**, *134*, 9082–9085.
- (16) Wu, X. L.; Wen, T.; Guo, H. L.; Yang, S.; Wang, X.; Xu, A. W. Biomass-Derived Sponge-like Carbonaceous Hydrogels and Aerogels for Supercapacitors. *ACS Nano* **2013**, *7*, 3589–3597.
- (17) Estevez, L.; Kelarakis, A.; Gong, Q.; Daas, E. H.; Giannelis, E. P. Multifunctional Graphene/Platinum/Nafion Hybrids via Ice Templating. *J. Am. Chem. Soc.* **2011**, *133*, 6122–6125.
- (18) Yan, Z.; Ma, L.; Zhu, Y.; Lahiri, I.; Myung Hahn, G.; Liu, Z.; Yang, S.; Xiang, C.; Lu, W.; et al. Three-Dimensional Metal Graphene Nanotube Multifunctional Hybrid Materials. *ACS Nano* **2013**, *7*, 58–64.
- (19) Chou, S. S.; De, M.; Luo, J.; Rotello, V. M.; Huang, J.; Dravid, V. P. Nanoscale Graphene Oxide (nGO) as Artificial Receptors: Implications for Biomolecular Interactions and Sensing. *J. Am. Chem. Soc.* **2012**, *134*, 16725–16733.
- (20) Yan, B.; Boyer, J. C.; Habault, D.; Branda, N. L.; Zhao, Y. Near Infrared Light Triggered Release of Biomacromolecules from Hydrogels Loaded with Upconversion Nanoparticles. *J. Am. Chem. Soc.* **2012**, *134*, 16558–16561.
- (21) Zhao, Y.; Hu, C.; Hu, Y.; Cheng, H.; Shi, G.; Qu, L. A Versatile, Ultralight, Nitrogen-Doped Graphene Framework. *Angew. Chem., Int. Ed.* **2012**, *51*, 11371–11375.
- (22) Zhu, Y.; Zhang, C.; Casillas, G.; Sun, Z.; Yan, Z.; Ruan, G.; Peng, Z.; Raji, A.-R. O.; Kittrell, C.; Hauge, R. H.; et al. A Seamless Three-Dimensional Carbon Nanotube Graphene Hybrid Material. *Nat. Commun.* **2012**, *3*, 1225–1228.
- (23) Qiu, L.; Liu, J. Z.; Chang, S. L. Y.; Wu, Y.; Li, D. Biomimetic Superelastic Graphene-Based Cellular Monoliths. *Nat. Commun.* **2012**, *3*, 1241.
- (24) Fan, Z.; Senapati, D.; Khan, S. A.; Singh, A. K.; Hamme, A.; Yust, B.; Sardar, D.; Ray, P. C. Popcorn-Shaped Magnetic Core–Plasmonic Shell Multifunctional Nanoparticles for the Targeted Magnetic Separation and Enrichment, Label-Free SERS Imaging, and Photothermal Destruction of Multidrug-Resistant Bacteria. *Chem.—Eur. J.* **2013**, *19*, 2839–2847.
- (25) Fan, Z.; Shelton, M.; Singh, A. K.; Senapati, D.; Khan, S. A.; Ray, P. C. Multifunctional Plasmonic Shell–Magnetic Core Nanoparticles for Targeted Diagnostics, Isolation, and Photothermal Destruction of Tumor Cells. *ACS Nano* **2012**, *6*, 1075–1083.
- (26) Singh, A. K.; Khan, S. A.; Fan, Z.; Demeritte, T.; Senapati, D.; Kanchanapally, R.; Ray, P. C. Development of a Long-Range Surface-Enhanced Raman Spectroscopy Ruler. *J. Am. Chem. Soc.* **2012**, *134*, 8662–8669.
- (27) Levin, C. S.; Hoffman, C.; Ali, T. A.; Kelly, A. T.; Morosan, E.; Nordlander, P.; Whitmire, K. H.; Halas, N. J. Magnetic–Plasmonic Core–Shell Nanoparticles. *ACS Nano* **2009**, *3*, 1379–1388.
- (28) Song, E.-Q.; Hu, J.; Wen, C.-Y.; Tian, Z.-Q.; Yu, X.; Zhang, Z.-L.; Shi, Y. B.; Pang, D. W. Fluorescent-Magnetic-Biotargeting Multifunctional Nanobioprobes for Detecting and Isolating Multiple Types of Tumor Cells. *ACS Nano* **2011**, *5*, 761–770.
- (29) Jung, N.; Crowther, A. C.; Kim, N.; Kim, P.; Brus, L. Raman Enhancement on Graphene: Adsorbed and Intercalated Molecular Species. *ACS Nano* **2010**, *4*, 7005–7013.
- (30) Ferrari, A. C.; Basko, D. M. Raman Spectroscopy as a Versatile Tool for Studying the Properties of Graphene. *Nat. Nanotechnol.* **2013**, *8*, 235–246.
- (31) Dasary, S. R.; Singh, A. K.; Senapati, D.; Yu, H.; Ray, P. C. Gold Nanoparticle Based Label-Free SERS Probe for Ultrasensitive and Selective Detection of Trinitrotoluene. *J. Am. Chem. Soc.* **2009**, *131*, 13806–13812.
- (32) Kim, N. H.; Lee, S. J.; Moskovits, M. Aptamer-Mediated Surface-Enhanced Raman Spectroscopy Intensity Amplification. *Nano Lett.* **2010**, *10*, 4181–4185.
- (33) Barhoumi, A.; Halas, N. J. Detecting Chemically Modified DNA Bases Using Surface-Enhanced Raman Spectroscopy. *J. Phys. Chem. Lett.* **2011**, *2*, 3118–3123.
- (34) Kleinman, S. L.; Ringe, E.; Valley, N.; Wustholz, K. L.; Phillips, E.; Scheidt, K. A.; Schatz, G. C.; Van Duyne, R. P. Single-Molecule Surface-Enhanced Raman Spectroscopy of Crystal Violet Isotopologues: Theory and Experiment. *J. Am. Chem. Soc.* **2011**, *133*, 4115–4122.
- (35) Murphy, S.; Huang, L.; Kamat, P. V. Reduced Graphene Oxide–Silver Nanoparticle Composite as an Active SERS Material. *J. Phys. Chem. C* **2013**, *117*, 4740–4747.
- (36) Brown, L. V.; Zhao, K.; King, N.; Sobhani, H.; Nordlander, P.; Halas, N. J. Surface-Enhanced Infrared Absorption Using Individual Cross Antennas Tailored to Chemical Moieties. *J. Am. Chem. Soc.* **2013**, *135*, 3688–3695.
- (37) Dijk, T.; Sivapalan, S. T.; DeVetter, B. M.; Yang, T. K.; Schulmerich, M. V.; Murphy, C. J.; Bhargava, R.; Carney, P. S. Competition between Extinction and Enhancement in Surface-Enhanced Raman Spectroscopy. *J. Phys. Chem. Lett.* **2013**, *4*, 1193–1196.
- (38) Patel, M.; Glass, R. I.; Jiang, B.; Santosh, M.; Lopman, B.; Parashar, U. A Systematic Review of Anti-Rotavirus Serum IgA Antibody Titer as a Potential Correlate of Rotavirus Vaccine Efficacy. *J. Infectious Disease* **2013**, *208*, 284–294.
- (39) Driskell, J. D.; Zhu, Y.; Kirkwood, C. D.; Zhao, Y.; Dluhy, R. A.; Tripp, R. A. Rapid and Sensitive Detection of Rotavirus Molecular Signatures Using Surface Enhanced Raman Spectroscopy. *PLoS One* **2010**, *5*, e10222.
- (40) Gutierrez, A. I.; Steyer, A.; Boben, J.; Gruden, K.; Poljsak, P. M.; Ravnikar, M. Sensitive Detection of Multiple Rotavirus Genotypes with a Single Reverse Transcription-Real-Time Quantitative PCR Sssay. *J. Clin. Microbiol.* **2008**, *46*, 2547–2554.
- (41) Logan, C.; O’Leary, J. J.; O’Sullivan, N. Real-Time Reverse Transcription-PCR for Detection of Rotavirus and Adenovirus as Causative Agents of Acute Viral Gastroenteritis in Children. *J. Clin. Microbiol.* **2006**, *44*, 3189–3195.